NANO LETTERS

2003
Vol. 3, No. 9
1299−1304

Mechanics of a Carbon Nanocoil

Xinqi Chen, Sulin Zhang, Dmitriy A. Dikin, Weiqiang Ding, and Rodney S. Ruoff*

Department of Mechanical Engineering, Northwestern University, Evanston, Illinois 60208

Lujun Pan and Yoshikazu Nakayama

Department of Physics and Electronics, Osaka Prefecture University, Sakai, Osaka 599-8531, Japan

Received June 2, 2003; Revised Manuscript Received June 23, 2003

ABSTRACT

An individual carbon nanocoil was clamped between two AFM cantilevers and loaded in tension to a maximum relative elongation of ~42%. The deformation of the nanocoil agrees well with an analytical model of the spring constant that accounts for the geometric nonlinearity. The nanocoil behaves like an elastic spring with a spring constant *K* of 0.12 N/m in the low strain region. No plastic deformation was detected. High-resolution microscopy images and the electron energy loss spectrum (EELS) indicate that the nanocoils are amorphous with a sp^2/sp^3 bonded-carbon ratio of ~4:1.

Carbon micro- and nanocoils have been synthesized and studied.[1−6] Because of their unique 3D structure, they have potential applications as mechanical components such as resonating elements and nanosprings or as a novel reinforcement in high-strain composites. Other potential applications are as nanosolenoids and electromagnetic wave absorbers. Volodin et al.[7] reported the elastic properties of coiled carbon nanotubes as measured with force modulation microscopy (an AFM technique). The tensile properties of helical diamond microfibers several millimeters in length and having a wire core of platinum have been discussed.[8] Nakayama et al.[9] presented a brief report on the mechanical properties of carbon nanocoils, and Motojima et al.[10] described the mechanical response of carbon microcoils under extension. Amorphous helical SiO_2 nanosprings have also been recently characterized by scanning and transmission electron microscopy and atomic force microscopy[11]. However, a direct experimental measurement of the mechanical response of carbon nanocoils under tensile loading has not yet been conducted and is the focus of the present study.

This carbon nanocoil was studied using a home-built nanomanipulator tool operated inside of a scanning electron microscope (SEM, LEO 1525). The nanocoil was picked up and then clamped between two AFM cantilever tips with the electron beam-induced deposition (EBID) method.[12,13] A loading experiment was conducted in which the nanocoil was monotonically loaded/unloaded in tension to a maximum coil extension of 33%. From the load versus elongation data, we have fit the spring constant (*K*) values for the nanocoil. (*k* is used later for the spring constant of the AFM cantilevers.) We derived an equation that expresses *K* in terms of the coil geometry and the shear modulus *G* and have used this equation to fit *G* from the measured values of *K* and the geometric parameters. In addition to our mechanical measurements, we present results of the structural analysis of other carbon nanocoils from the same sample, as obtained by transmission electron microscopy (TEM, Hitachi HF-2000 and Hitachi H-8100).

The carbon nanocoils were synthesized with catalytic thermal chemical vapor deposition (CVD) by the coauthors from Osaka Prefecture University,[5] and all mechanical testing and structural analysis was performed by the Northwestern University team. A metal wire covered with adhesive carbon tape was used to touch the nanocoil sample, which caused some nanocoils to adhere to the tape surface. This tape was then used as a nanocoil source for our mechanical measurements. Figure 1 shows an SEM image of various carbon nanocoils grown from an iron-coated indium tin oxide (ITO) thin film deposited on a glass substrate as well as a schematic of the tensile loading experiment.

For the tensile loading experiment, two ultrasharp AFM cantilevers from Mikromasch, Inc. were mounted on the nanomanipulator. A stiff AFM cantilever (chip NSC12; we used the longest of the six cantilevers on the chip with a spring constant of $k \approx 0.1$ to 0.4 N/m provided by Mikromasch) is attached to one end of the nanocoil. The deformation of the compliant AFM cantilever (chip CSC12; we again used the longest cantilever on the chip, with $k \approx 0.01$ to 0.08 N/m as quoted by the manufacturer) is used as a force-sensing element. The applied force is calculated from the observed deflection of the soft cantilever, and the nanocoil elongation is determined from the acquired SEM images.

A typical mounting operation involves approaching an individual nanocoil with the rigid cantilever tip and then

* Corresponding author. E-mail: r-ruoff@northwestern.edu. Tel: 847-467-6596. Fax: 847-491-3915.

10.1021/nl034367o CCC: $25.00
Published on Web 08/08/2003

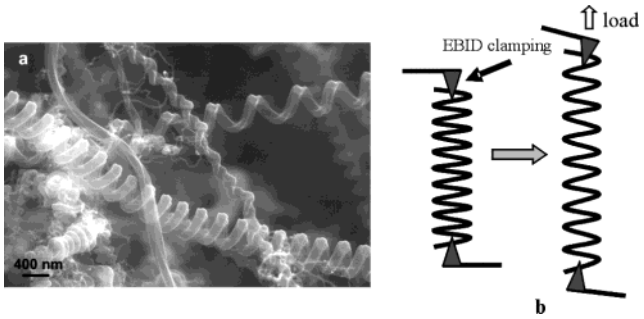

Figure 1. (a) SEM image of carbon nanocoils. (b) Schematic of tensile loading of an individual nanocoil.

creating a clamp on the tip by EBID of residual hydrocarbons in the SEM environment. The desire to extract an individual nanocoil for subsequent mounting onto the opposing cantilever tip was typically thwarted because of the extension of the nanocoil to a certain point, followed by violent detachment that often resulted in the loss of the nanocoil because of its having "sprung away." The nanocoil that is the subject of this paper was actually first studied by extending it with respect to the source (the tape on the metal wire). We were fortunate to succeed in freeing it from the substrate at an elongation of ~42%, as measured by the relative displacement between six turns in the nanocoil as shown in Figure 2, without the clamp failing at the tip. We note that this carbon nanocoil returned completely to its relaxed geometry after loading without apparent plastic deformation.

Once the nanocoil was freed from the source as described above, the more compliant cantilever tip was brought into contact with the opposite end of the nanocoil and attached via another EBID clamp. The nanocoil was then subject to tensile loading by applying a series of discrete voltages to a piezoelectric multilayer bender (Noliac A/S, Denmark, ceramic multilayer bender B1) as shown in Figure 3, where the cantilever on the left is the stiffer cantilever and the one on the right is the more compliant cantilever. The displacement of the more compliant cantilever, with a spring constant of $k = 0.047 \pm 0.003$ N/m, was used to measure the applied load. (We discuss the calibration of the AFM cantilevers below.) Also shown in Figure 3 are images of the nanocoil at 20% and 33% relative elongation. After reaching the maximum 33% relative elongation, the load was slowly released, and the nanocoil relaxed to its original length and geometry. Again, no plastic deformation was identified after the nanocoil was unloaded.

Previously, a method that we use for measuring small (ranging from fractions of a micro-Newton to micro-Newtons) applied forces from small cantilever deflections[14] has been described. The displacement of the relatively soft cantilever AFM tip was calibrated as a function of the voltage applied to the piezoelectric bender. The displacement of the tip both with and without the nanocoil was measured with the same potential (volts) applied to the piezoelectric bender. The difference between the two displacements is the true deflection of the AFM cantilever. This method allows accurate measurements of small displacements by tracking the AFM tip position at the highest SEM magnification.

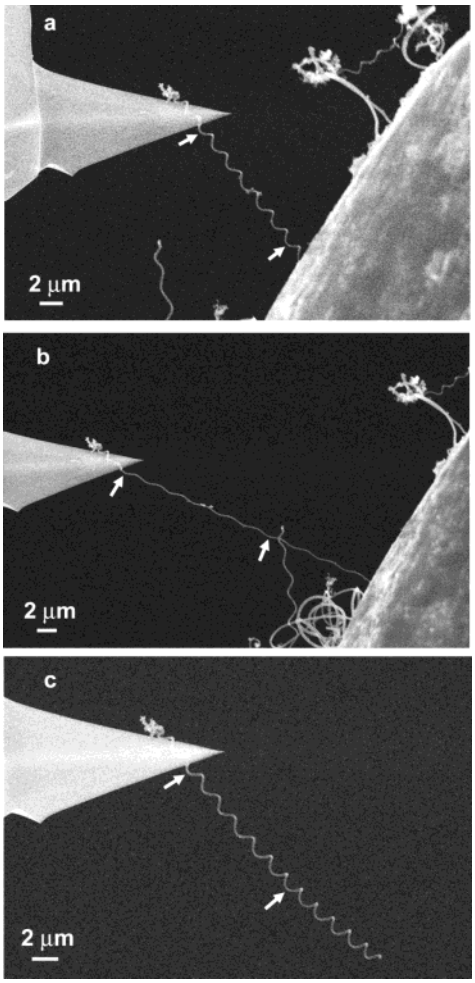

Figure 2. (a) Nanocoil picked up by the AFM tip. (b) Nanocoil extension upon extraction from the substrate. (c) Nanocoil detachment from the substrate. The distance between the six turns is, within experimental error, identical to the equivalent distance in (a).

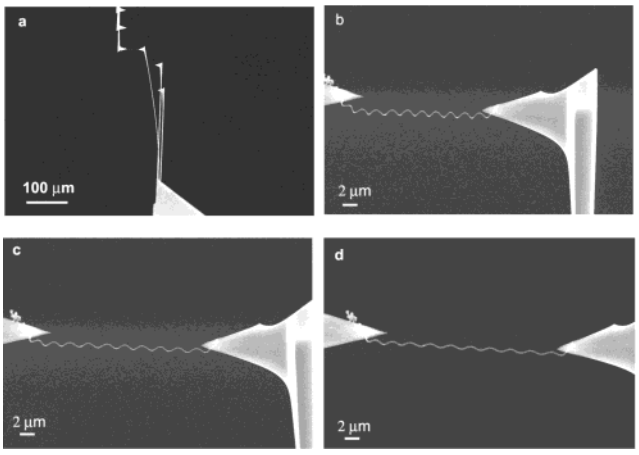

Figure 3. (a) Nanocoil clamped between two AFM cantilevers. The left cantilever is stiffer than the right cantilever. (b) Relaxed nanocoil prior to loading. (c) Nanocoil at a relative elongation of 20%. (d) Nanocoil at a relative elongation of 33%.

The spring constant of each cantilever was calibrated before the tensile loading experiment. The calibration procedure is based on the method reported in ref 15. The resonance frequency of each cantilever and all of the

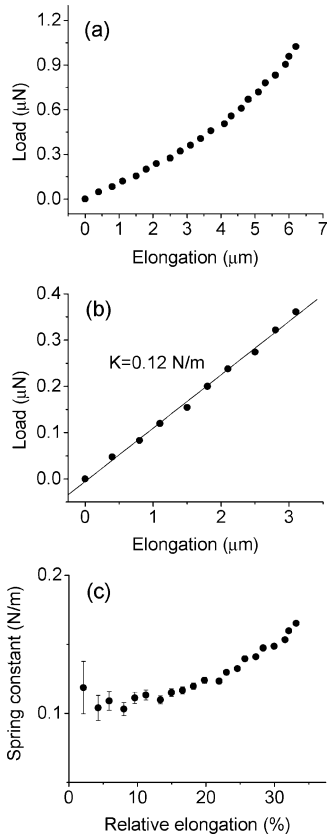

Figure 4. (a) Load versus elongation response of the nanocoil. (b) Low-strain region response. (c) Spring constant versus the relative elongation. The spring constant values are obtained from the load versus elongation data in (a).

cantilever dimensions were measured inside of the SEM. The spring constant k is $k = M_e\rho_c bhL\omega_{vac}^2$, where M_e is the normalized effective mass, ρ_c is the cantilever mass density, b, h, and L are the width, the thickness, and the length of the cantilever beam, respectively, and ω_{vac} is the natural resonance frequency in vacuum ($\omega_{vac} = 2\pi f_{vac}$).[15] The geometry of the soft cantilever as measured in the SEM was $b = 35 \pm 0.5$ μm, $h = 1.0 \pm 0.05$ μm, and $L = 350 \pm 5$ μm. From the measured $f_{vac} = 13.1 \pm 0.1$ kHz and by assuming that $\rho_c = 2.33$ g/cm^3 and setting M_e equal to 0.2427 as discussed in the literature,[15] we find that the spring constant k of the soft cantilever is 0.047 ± 0.003 N/m. The applied load is given by the spring constant of the cantilever multiplied by its deflection.

The spring constant K of the nanocoil is defined as the total applied load divided by the total elongation. The spring constants of the nanocoil at discrete elongations were calculated and are plotted in Figure 4. From the low-elongation data (see Figure 4b), a linear fit value for K of 0.12 N/m is obtained. Figure 4c illustrates the measured spring constant K versus the relative elongation of the nanocoil. It indicates that the spring constant of the nanocoil increases with increasing relative elongation. To explain this result, the nanocoil has been analyzed in terms of the mechanics of a helical spring as described below.

The spring constant K of a helical spring is a function of the geometry and shear modulus of the material and can be

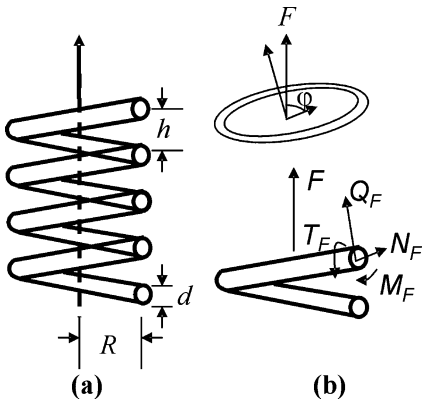

Figure 5. (a) Schematic representation of the nanocoil as a helical spring. (b) Resultant forces at the cross section of the nanocoil.

expressed as[16,17]

$$K = \frac{Gd^4}{64R^3N} \tag{1}$$

where d is the diameter of the coil wire, G *is* the shear modulus, R is the radius of the coil, and N is the number of coils. The above equation takes into account only the torsion generated from the extension of the spring and hence is accurate only in the low-strain regime. When the spring is in the high-strain region, the contributions from the bending, shear, and tension may not be negligible. In what follows, a more accurate expression is presented.

Because of the symmetric geometry of the coil spring, only one unit cell is considered in the following analysis, as shown in Figure 5. When subjected to a pure axial tensile load defined as F, the axial stretch of the unit cell Δ can be determined by using the principle of virtual work:[18]

$$\Delta = \int_0^l \frac{N_u N_F}{EA}\,ds + \int_0^l \frac{\alpha_s Q_u Q_F}{GA}\,ds + \int_0^l \frac{M_u M_F}{EI}\,ds + \int_0^l \frac{T_u T_F}{GJ}\,ds \tag{2}$$

where l is the total length of the unit cell, α_s is the shear coefficient, E is the tensile modulus, A is the cross-sectional area of the coil wire, I is the moment of inertia, and J is the polar moment of inertia of the cross section. The variables N_u, Q_u, M_u, and T_u are the axial force, shear force, bending moment, and torsion, respectively, caused by a unit tensile load of $P_u = 1$ along the axial direction. N_F, Q_F, M_F, and T_F are the tension, shear, bending moment, and torsion, respectively, caused by the applied tensile force F.

An arbitrary point along the central line of the unit cell has spatial coordinates of $[R\cos\theta, R\sin\theta, (h/2\pi)\theta]$, where θ is the radial angle ranging from 0 to 2π and h the height of the unit cell. The tangential direction at this point is then $(-R\sin\theta, R\cos\theta, h/2\pi)$. The length of unit cell is thus $l = 2\pi\sqrt{R^2+H^2}$, where $H = h/2\pi$. We assume that l is constant. Denoting φ as the angle between the tangential direction and the axial direction of the coil gives $\cos\varphi =$

$H/\sqrt{R^2+H^2}$. Thus, the tension, shear, torsion, and bending at the cross section of the coil can be expressed as

$$\text{tension: } N_F = F \cdot \cos\varphi = \frac{FH}{\sqrt{R^2+H^2}}$$

$$\text{shear: } Q_F = F \cdot \sin\varphi = \frac{FR}{\sqrt{R^2+H^2}}$$

$$\text{bending: } M_F = F \cdot \cos\varphi \cdot R = \frac{FRH}{\sqrt{R^2+H^2}}$$

$$\text{torsion: } T_F = F \cdot \sin\varphi \cdot R = \frac{FR^2}{\sqrt{R^2+H^2}}$$

Then, eq 2 can be rewritten as follows:

$$\Delta = \frac{FH^2}{R^2+H^2}\cdot\frac{l}{EA} + \frac{\alpha_s FR^2}{R^2+H^2}\cdot\frac{l}{GA} + \frac{FR^2H^2}{R^2+H^2}\cdot\frac{l}{EI} + \frac{FR^4}{R^2+H^2}\cdot\frac{l}{GJ} \quad (3)$$

We define $K = F/\Delta$ such that

$$\frac{1}{K} = \frac{H^2}{R^2+H^2}\cdot\frac{l}{EA} + \frac{\alpha_s R^2}{R^2+H^2}\cdot\frac{l}{GA} + \frac{R^2H^2}{R^2+H^2}\cdot\frac{l}{EI} + \frac{R^4}{R^2+H^2}\cdot\frac{l}{GJ} \quad (4)$$

where $\alpha_s = (7 + 6\upsilon)/6(1 + \upsilon)$ and υ is Poisson's ratio. If the unit coil is extended as Δ, then $H = (h + \Delta)/2\pi$ and $R = \sqrt{[l^2-(h+\Delta)^2]/(2\pi)^2}$.

For a coil wire of circular cross section,

$$A = \frac{\pi d^2}{4} \qquad I = \frac{\pi d^4}{64} \qquad J = \frac{\pi d^4}{32}$$

By substituting the above expressions into eq 4, one has

$$\frac{1}{K} = \frac{8H^2}{Ed^2\sqrt{R^2+H^2}} + \frac{8\alpha_s R^2}{Gd^2\sqrt{R^2+H^2}} + \frac{128R^2H^2}{Ed^4\sqrt{R^2+H^2}} + \frac{64R^4}{Gd^4\sqrt{R^2+H^2}} \quad (5)$$

where $E = 2(1 + \nu)G$. We define $\beta = 2(1 + \upsilon)$. Then,

$$K = \frac{Gd^4}{64R^3}\frac{1}{\xi} \quad (6)$$

where ξ is a dimensionless coefficient that describes the geometry of the coil,

$$\xi = \frac{H^2d^2}{8\beta R^3\sqrt{R^2+H^2}} + \frac{\alpha_s d^2}{8R\sqrt{R^2+H^2}} + \frac{2H^2}{\beta R\sqrt{R^2+H^2}} + \frac{R}{\sqrt{R^2+H^2}} \quad (7)$$

For coil springs that are composed of N turns, eq 6 can be rewritten as

$$K = \frac{Gd^4}{64R^3N}\cdot\frac{1}{\xi} \quad (8)$$

For a coiled nanotube with outer diameter d_1 and inner diameter d_2, eq 8 can be rewritten as

$$K = \frac{G({d_1}^4 - {d_2}^4)}{64R^3N}\cdot\frac{1}{\xi} \quad (9)$$

where ξ is expressed as:

$$\xi = \frac{H^2({d_1}^2 + {d_2}^2)}{8\beta R^3\sqrt{R^2+H^2}} + \frac{\alpha_s({d_1}^2 + {d_2}^2)}{8R\sqrt{R^2+H^2}} + \frac{2H^2}{\beta R\sqrt{R^2+H^2}} + \frac{R}{\sqrt{R^2+H^2}} \quad (10)$$

Equations 8 and 9 take into account the nonlinear relationship between the shear modulus and the set of measured spring constants. Hence, it is valid as long as the deformation of the coil spring remains in the elastic regime. In the limiting case $R \gg H$, the first three terms on the right side of eq 7 are negligible compared with the fourth term, leading to the simplified case described by eq 1. However, if $R \ll H$, then eq 8 is reduced to the case of uniaxial elongation of a straight beam.

We consider two examples to discuss the above analysis. The first example is a unit nanocoil with $d = 120$ nm, $R = 420$ nm, $h = 120$ nm, $G = 2.5$ GPa, $\upsilon = 0.27$, and a very small helical angle. Figure 6a plots the spring constant versus relative elongation based on eq 6. It indicates that the spring constant remains constant even though the relative elongation exceeds 30%. Figure 6b shows the contribution to the spring constant from the tension, bending, shear, and torsion generated by the extension of the coil based on eq 7. It clearly shows that torsion dominates the response and that the contributions from the tension, bending, and shear components are negligible. For the second example, we consider a nanocoil with a larger helical angle for which $h = 2000$ nm and the rest of the parameters are the same as in the first case. Parts c and d of Figure 6 show the plot of the spring constant versus relative elongation and the percentage contribution to the spring constant from the tension, bending, shear, and torsion generated by the extension of the coil. The results show that the spring constant will increase as

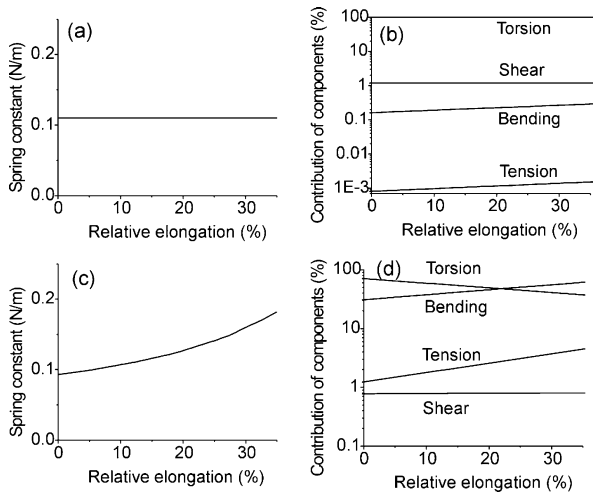

Figure 6. Analytical modeling of the spring constant of a nanocoil. For a small helical angle: (a) spring constant versus relative elongation and (b) contribution of spring constant components versus relative elongation. For a large helical angle: (c) spring constant versus relative elongation and (d) contribution of spring constant components versus relative elongation.

the coil is extended even though the relative elongation is less than 30%. In this case, both the bending and the torsion contribute significantly to the response. The bending contribution increases and the torsion contribution decreases with increasing relative elongation.

The experimental nanocoil behavior discussed earlier is similar to the second example. According to eq 8, as the nanocoil is elongated under pure tensile load, the coil radius R decreases, and the spring constant increases because the other variables such as coil wire diameter d and shear modulus G are assumed to be constant in this analysis. From the comparison between Figures 4c and 6c, it is clear that the experimental data are consistent with this theoretical analysis.

The growth mechanism of carbon nanocoils has been discussed in the literature.[19] The catalyst is located at the tip of the nanocoil, indicating a tip-growth mechanism. The TEM diffraction pattern shown in the inset of Figure 7a was taken using another carbon nanocoil and demonstrates that it is amorphous. As shown in Figure 7, SEM and TEM images indicate that most of the nanocoils consist of more than one wire and typically have a double-helical structure. In addition, the TEM image in Figure 7a shows that each wire of the nanocoil is hollow.

Figure 7b shows a relatively high magnification SEM image of the nanocoil that was mechanically loaded, and the inset of Figure 7b shows a schematic of a double coil. As mentioned above, this nanocoil was stretched several times, and even though the relative elongation reached 42%, no separation or sliding between the two wires was observed. This suggests that the two wires are tightly joined. Thus, for purposes of modeling, we assume that the cross section of the nanocoil is two joined tubes. The outer diameter (o.d.) of each tube is $\sim 126 \pm 4$ nm, as measured from the SEM image. Although the inner diameter (i.d.) of this particular nanocoil is unknown, below we consider a few different

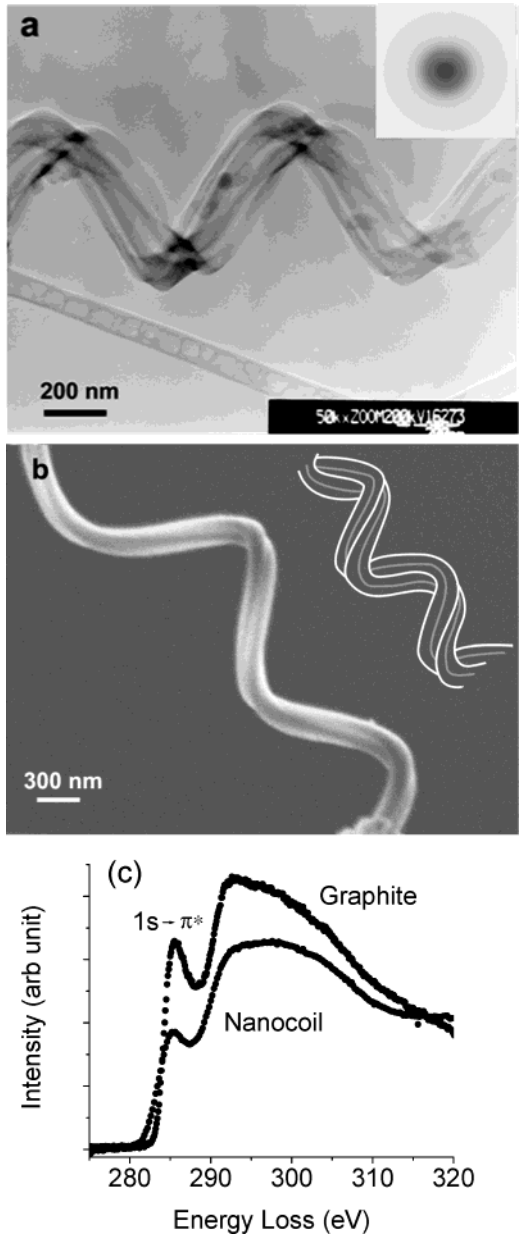

Figure 7. (a) Transmission electron microscopy image of a carbon nanocoil. Inset: TEM diffraction pattern taken from this nanocoil (both obtained in a Hitachi H-8100 TEM). (b) High-magnification SEM image of the nanocoil used in the tension experiments (Leo 1525 SEM). Inset: schematic of a double coil. (c) Electron energy loss spectrum of a different carbon nanocoil obtained using a Hitachi HF-2000.

cases. If the i.d. = 3/4 that of the o.d., then the shear modulus G fitted according to eq 4 is $\sim 2.5 \pm 0.4$ GPa, which is the mean value of the 21 G values fit to the 21 measured (K, elongation) points. If i.d. = 1/2 o.d., then the mean value of G is $\sim 2.3 \pm 0.4$ GPa, and for two joined (solid) wires (i.d. = 0), the mean value of G will be $\sim 2.1 \pm 0.3$ GPa. Thus, the value of G does not depend very strongly on the inner diameter of the individual tubes. These results indicate that the shear modulus G of the carbon nanocoil is *much* lower than that of carbon nanotubes for which a shear modulus of roughly 400 GPa has been estimated.[20] A future area of study

is the graphitization of the carbon nanocoils to enhance their mechanical properties.

The electron energy loss spectrum (EELS) of the carbon nanocoils was obtained with a Hitachi HF2000 at 200 keV as shown in Figure 7c. Carbon was the only element detected in the nanocoil. (It is difficult to detect hydrogen with EELS.) To get the sp^2/sp^3 ratio of the nanocoil sample, a graphite sample was used as a reference for pure sp^2 bonding. The graphite sample was prepared by cleaving fragments from a bulk specimen of highly oriented pyrolytic graphite (HOPG). The HOPG fragments were ground into fine powder using a mortar and pestle and dispersed in acetone. One drop of this suspension was put on a lacey carbon grid so that after drying many graphite platelets were attached to the grid. Because the graphite is anisotropic, the observed intensity depends on the orientation of the beam with respect to the graphite layer; here the spectrum was recorded with the beam parallel to the graphite layer. EELS data were taken in diffraction mode for two independent nanocoils and analyzed according to the method described in the literature.[21,22] The atomic fraction of sp^2-bonded carbon for these two nanocoils was $\sim$0.8.

In conclusion, a carbon nanocoil was loaded in tension inside of a scanning electron microscope. The nanocoil behaves like an elastic spring with a spring constant K of 0.12 N/m in the low-strain regime, with an upturn in K in the high-strain regime. The mechanical properties of the nanocoil were characterized on the basis of a nonlinear relationship between the spring constant K of the nanocoil and the shear modulus G in which the contributions of all of the components of the restoring force are included. Several nanocoils in the sample were characterized by transmission electron microscopy images and diffraction patterns and electron energy loss spectroscopy. The results indicate that the nanocoils are double- (and even in some cases triple-) coiled amorphous carbon nanotubes having a relatively high sp^2 bonding content.

Acknowledgment. We gratefully acknowledge the Mechanics of Nanostructures grant (award no. N000140210870) from the Office of Naval Research, the NASA University Research, Engineering and Technology Institute on Bio Inspired Materials (BIMat) under award no. NCC-1-02037, and the NASA Langley Computational Materials Nanotechnology Program. We appreciate the use of the Northwestern University Electron Probe Instrumentation Center (EPIC) facilities and the assistance of Shuyou Li with the EELS experiments. We also thank Frank Fisher and Gregory J. Wagner for helpful comments.

References

(1) Davis, W. R.; Slawson, R. J.; Rigby, G. R. *Nature* **1953**, *171*, 756.
(2) Radlein, D.; Whitehead, J. C.; Grice, R. *Nature* **1975**, *253*, 37.
(3) Motojima, S.; Kawaguchi, M.; Nozaki, K.; Iwanaga, H. *Carbon* **1991**, *29*, 379.
(4) Kuzuya, C.; Wan, I.; Hirako, S.; Hishikawa, Y.; Motojima, S. *Chem. Vap. Deposition* **2002**, *8*, 57.
(5) Zhang, M.; Nakayama, Y.; Pan, L. *Jpn. J. Appl. Phys., Part 2* **2000**, *39*, L1242.
(6) Varadan, V. K.; Xie, J. *Smart Mater. Struct.* **2002**, *11*, 728.
(7) Volodin, A.; Ahlskog, M.; Seynaeve, E.; Haesendonck, C. V.; Fonseca, A.;. Nagy, J. B. *Phys. Rev. Lett.* **2000**, *84*, 3342.
(8) Partridge, P. G.; Humberstone, L.; Doble, J. B.; Gilmore, C. J.; Ubhi, H. S. *Mater. Sci. Technol.* **1999**, *15*, 1101.
(9) Hayashida, T.; Pan, L.; Nakayama, Y. *Physica B* **2002**, *323*, 352.
(10) Motojima, S.; Kawaguchi, M.; Nozaki, K.; Iwanaga, H. *Appl. Phys. Lett.* **1990**, *56*, 321.
(11) Zhang, H. F.; Wang, C. M.; Buck, E. C.; Wang, L. S. *Nano Lett.* **2003**, *3*, 577.
(12) Yu, M. F.; Dyer, M. J.; Skidmore, G. D.; Rohrs, H. W.; Lu, X. K.; Ausman, K. D.; Von Her, J. R.; Ruoff, R. S. *Nanotechnology* **1999**, *10*, 244.
(13) Yu, M. F.; Lourie, O.; Dyer, M. J.; Moloni, K.; Kelly, T. F.; Ruoff, R. S. *Science* **2000**, *287*, 637.
(14) Yu, M. F.; Files, B. S.; Arepalli, S.; Ruoff, R. S. *Phys. Rev. Lett.* **2000**, *84*, 5552.
(15) Sader, J. E.; Larson, I.; Mulvaney, P.; White, L. R. *Rev. Sci. Instrum.* **1995**, *66*, 3789.
(16) Granet, I. *Strength of Materials for Engineering Technology*, 2nd ed.; Reston Publishing Company: Reston, VA, 1980.
(17) Wahl, A. M. *Mechanical Springs*, 2nd ed.; McGraw-Hill: New York, 1963.
(18) Timoshenko, S.; Gere, J. *Mechanics of Materials*; Van Nostrand Reinhold Company: New York, 1972.
(19) Pan, L.; Zhang, M.; Nakayama, Y. *J. Appl. Phys.* **2002**, *91*, 10058.
(20) Lu, J. P. *Phys. Rev. Lett.* **1997**, *79*, 1297.
(21) Cuomo, L. J.; Doyle, J. P.; Bruley, J.; Liu, J. C. *Appl. Phys. Lett.* **1991** *58*, 466.
(22) Kulik, J.; Lifshitz, Y.; Lempert, G. D.; Rabalais, J. W.; Marton, D. *J. Appl. Phys.* **1994**, *76*, 5063.

NL034367O